Inorg. Chem. **2007**, *46*, 11082–11093

Blue-Emitting Iridium Complexes with Substituted 1,2,4-Triazole Ligands: Synthesis, Photophysics, and Devices

Enrico Orselli,[†,‡] Gregg S. Kottas,*[,†,‡] Asgeir E. Konradsson,[†,‡] Paolo Coppo,[§] Roland Fröhlich,[||] Luisa De Cola,*[,†,‡] Addy van Dijken,[⊥] Michael Büchel,[⊥] and Herbert Börner[¥]

Westfälische Wilhelms-Universität Münster, Physikalisches Institut, Mendelstrasse 7, 48149 Münster, Germany, Center for Nanotechnology (CeNTech), Heisenbergstrasse 11, 48149 Münster, Germany, Wolfson Centre for Materials Processing, Brunel University, Uxbridge, Middlesex UB8 3PH, United Kingdom, Westfälische Wilhelms-Universität Münster, Organisch-Chemisches Institut, Corrensstrasse 40, 48149 Münster, Germany, Philips Research, Philips Natuurkundig Laboratorium, Prof. Holstlaan 4, 5656 AA Eindhoven, The Netherlands, and Philips Research Labs, Weisshausstrasse 2, 52066 Aachen, Germany

Received June 6, 2007

Neutral heteroleptic mononuclear iridium(III) complexes with (2,4-difluoro)phenylpyridine and different pyridine-1,2,4-triazole ligands were synthesized and fully characterized. We investigated the effects of substituents in the 5-position of the triazole ring on the photophysical and electrochemical behavior. Increasing the electron-withdrawing capabilities generally leads to a lowering of the HOMO level with a consequent slight widening of the HOMO–LUMO gap and a blue shift in emission. The complexes reported exhibit high emission quantum yields and long luminescent lifetimes, typical of iridium(III) complexes, and most of them show reversible redox processes in solution. Also, many of the complexes reported here have been obtained as single crystals suitable for X-ray crystallography. Two of the complexes were further tested as phosphorescent dyes in OLED devices and showed high external quantum efficiencies (~7%) and color points better than the "standard" for blue iridium(III) bis[(4,6-difluorophenyl)-pyridinato-*N*,$C^{2'}$]picolinate (FIrpic). We also report the full electrochemical investigation of FIrpic in different solvents.

Introduction

Iridium(III) organometallic complexes have received a great deal of interest in a variety of photonic applications. In particular, the charged compounds have been intensely studied for use as dopants in light-emitting electrochemical cells (LEECs)[1,2] and the neutral ones in organic/organometallic light-emitting diodes (OLEDs).[1−3] Iridium(III), as other heavy transition metals like ruthenium, osmium, and platinum, harvests both singlet and triplet states from electrically generated excitons, leading to theoretical efficiencies of 100%, whereas fluorescent molecules can only utilize the singlet excitons and thus have a maximum theoretical efficiency of 25%.[3−5] Also, its ambipolar character, with an oxidation mainly involving the metal and a reduction on the coordinating ligands, allows the charge recombination to occur on the metal complex with formation of a luminescent excited state.

Of special interest for Ir(III) complexes is the color tunability of the emission from red[6−8] to green[1] and, in particular, blue.[9−21] The ability to cover the entire visible emission spectrum has further led to use of Ir(III) complexes

* To whom correspondence should be addressed. E-mail: decola@uni-muenster.de and kottas@uni-muenster.de.
† Westfälische Wilhelms-Universität Münster, Physikalisches Institut.
‡ Center for Nanotechnology (CeNTech).
§ Brunel University.
|| Westfälische Wilhelms-Universität Münster, Organisch-Chemisches Institut.
⊥ Philips Research, The Netherlands.
¥ Philips Research Labs, Germany.

(1) Holder, E.; Langeveld, B. M. W.; Schubert, U. S. *Adv. Mater.* **2005**, *17*, 1109−1121.
(2) Chou, P.-T.; Chi, Y. *Chem. Eur. J.* **2007**, *13*, 380−395.
(3) Yersin, H. *Top. Curr. Chem.* **2004**, *241*, 1−26.
(4) Baldo, M.; Segal, M. *Phys. Status Solidi A* **2004**, *201*, 1205−1214.
(5) Baldo, M. A.; O'Brien, D. F.; You, Y.; Shoustikov, A.; Sibley, S.; Thompson, M. E.; Forrest, S. R. *Nature* **1998**, *395*, 151−154.
(6) Tsuboyama, A.; Iwawaki, H.; Furugori, M.; Mukaide, T.; Kamatani, J.; Igawa, S.; Moriyama, T.; Miura, S.; Takiguchi, T.; Okada, S.; Hoshino, M.; Ueno, K. *J. Am. Chem. Soc.* **2003**, *125*, 12971−12979.
(7) Liang, B.; Jiang, C. Y.; Chen, Z.; Zhang, X. J.; Shi, H. H.; Cao, Y. *J. Mater. Chem.* **2006**, *16*, 1281−1286.
(8) Liu, Z. W.; Guan, M.; Bian, Z. Q.; Nie, D. B.; Gong, Z. L.; Li, Z. B.; Huang, C. H. *Adv. Funct. Mater.* **2006**, *16*, 1441−1448.

10.1021/ic701110p CCC: $37.00
Published on Web 11/21/2007

in LEDs producing white light.[22−34] The color tunability is due to the fact that the emitting excited state is a triplet level that can be a metal-to-ligand charge-transfer state (MLCT) or, which is more often the case for high-energy emitting species, a mixed state with MLCT and ligand-centered (LC) character.[14,35−37] In general, the luminescent properties of Ir(III) complexes are strongly related to the sigma-donating and electron-accepting capabilities of the coordinating ligands allowing, to a certain extent, prediction and design of the properties of the complexes.[14] For the common 2-phenylpyridine (ppy) ligand, as in the prototypical green-emitting phosphor $Ir(ppy)_3$, the emissive state is believed to be from a HOMO that is localized on phenyl π and iridium d orbitals, while the LUMO is localized on the π^* orbitals of the pyridine ring.[38,39] Therefore, there are several strategies developed to shift the emission to the blue: (a) addition of electron-withdrawing groups to the phenyl rings coordinated to the metal ion to stabilize the HOMO and thus increase the HOMO−LUMO gap,[10−12,15,21,40] which has proven successful to obtain 'sky blue' emission, (b) changing ancillary ligands coordinated to Ir(III) from aromatic groups to cyano[40−42] and isocyanide[43] derivatives as strong electron-withdrawing groups, and destabilizing the LUMO by (c) addition of electron-donating groups to the pyridine ring[15,44−46] or (d) using strong σ-donating ligands such as carbenes.[14] This last approach was extremely successful in producing complexes that emit 'true blue' light and even into the near-UV. The luminescence quantum yields in these first-generation complexes were, however, quite modest.

In this publication, we report on heteroleptic Ir(III) complexes that give sky-blue emission (∼460 nm) with high emission quantum yields in fluid solution at room temperature. The complexes bear two 4,6-difluorophenylpyridine ligands and a third (1,2,4-triazol-3-yl)pyridine ancillary ligand with different substituents in the 5-position. Previous reports have investigated the effects of changing the substitution of the phenylpyridine ligand in related complexes,[10,15] but to the best of our knowledge, only scattered examples of triazole derivatives have been reported.[18,47,48] Therefore, for a better understanding of the effects of such substituents, we attempt to systematically alter the photophysical properties by selectively changing the substituents on the (1,2,4-triazol-3-yl)pyridine ligand. In general, azole ligands are typically strong σ-donor and weak π-acceptor ligands due to the electron-rich nature of the five-membered aromatic ring.[49] In particular, 1,2,4-triazoles are of interest due to the deprotonation of the azole ring upon coordination, and in our case, this formally anionic nitrogen leads to a neutral iridium complex.

(9) Adachi, C.; Kwong, R. C.; Djurovich, P.; Adamovich, V.; Baldo, M. A.; Thompson, M. E.; Forrest, S. R. *Appl. Phys. Lett.* **2001**, *79*, 2082−2084.
(10) Coppo, P.; Plummer, E. A.; De Cola, L. *Chem. Commun.* **2004**, 1774−1775.
(11) Dedeian, K.; Shi, J. M.; Shepherd, N.; Forsythe, E.; Morton, D. C. *Inorg. Chem.* **2005**, *44*, 4445−4447.
(12) Grushin, V. V.; Herron, N.; LeCloux, D. D.; Marshall, W. J.; Petrov, V. A.; Wang, Y. *Chem. Commun.* **2001**, 1494−1495.
(13) Holmes, R. J.; Forrest, S. R.; Tung, Y. J.; Kwong, R. C.; Brown, J. J.; Garon, S.; Thompson, M. E. *Appl. Phys. Lett.* **2003**, *82*, 2422−2424.
(14) Sajoto, T.; Djurovich, P. I.; Tamayo, A.; Yousufuddin, M.; Bau, R.; Thompson, M. E.; Holmes, R. J.; Forrest, S. R. *Inorg. Chem.* **2005**, *44*, 7992−8003.
(15) Takizawa, S.; Echizen, H.; Nishida, J.; Tsuzuki, T.; Tokito, S.; Yamashita, Y. *Chem. Lett.* **2006**, *35*, 748−749.
(16) Tamayo, A. B.; Alleyne, B. D.; Djurovich, P. I.; Lamansky, S.; Tsyba, I.; Ho, N. N.; Bau, R.; Thompson, M. E. *J. Am. Chem. Soc.* **2003**, *125*, 7377−7387.
(17) Tokito, S.; Iijima, T.; Suzuri, Y.; Kita, H.; Tsuzuki, T.; Sato, F. *Appl. Phys. Lett.* **2003**, *83*, 569−571.
(18) Yang, C. H.; Li, S. W.; Chi, Y.; Cheng, Y. M.; Yeh, Y. S.; Chou, P. T.; Lee, G. H.; Wang, C. H.; Shu, C. F. *Inorg. Chem.* **2005**, *44*, 7770−7780.
(19) Yeh, S. J.; Wu, M. F.; Chen, C. T.; Song, Y. H.; Chi, Y.; Ho, M. H.; Hsu, S. F.; Chen, C. H. *Adv. Mater.* **2005**, *17*, 285−289.
(20) Yang, C. H.; Cheng, Y. M.; Chi, Y.; Hsu, C. J.; Fang, F. C.; Wong, K. T.; Chou, P. T.; Chang, C. H.; Tsai, M. H.; Wu, C. C. *Angew. Chem., Int. Ed.* **2007**, *46*, 2418−2421.
(21) Ragni, R.; Plummer, E. A.; Brunner, K.; Hofstraat, J. W.; Babudri, F.; Farinola, G. M.; Naso, F.; De Cola, L. *J. Mater. Chem.* **2006**, *16*, 1161−1170.
(22) Cheng, G.; Zhang, Y. F.; Zhao, Y.; Liu, S. Y.; Ma, Y. G. *Appl. Phys. Lett.* **2006**, *88*, 083512.
(23) Coppo, P.; Duati, M.; Kozhevnikov, V. N.; Hofstraat, J. W.; De Cola, L. *Angew. Chem., Int. Ed.* **2005**, *44*, 1806−1810.
(24) D'Andrade, B. W.; Forrest, S. R. *Adv. Mater.* **2004**, *16*, 1585−1595.
(25) D'Andrade, B. W.; Holmes, R. J.; Forrest, S. R. *Adv. Mater.* **2004**, *16*, 624−628.
(26) Gong, X.; Wang, S.; Moses, D.; Bazan, G. C.; Heeger, A. J. *Adv. Mater.* **2005**, *17*, 2053−2058.
(27) Kanno, H.; Holmes, R. J.; Sun, Y.; Kena-Cohen, S.; Forrest, S. R. *Adv. Mater.* **2006**, *18*, 339−342.
(28) Krummacher, B. C.; Choong, V. E.; Mathai, M. K.; Choulis, S. A.; So, F.; Jermann, F.; Fiedler, T.; Zachau, M. *Appl. Phys. Lett.* **2006**, *88*, 113506.
(29) Lei, G. T.; Wang, L. D.; Qiu, Y. *Appl. Phys. Lett.* **2004**, *85*, 5403−5405.
(30) Sun, Y. R.; Giebink, N. C.; Kanno, H.; Ma, B. W.; Thompson, M. E.; Forrest, S. R. *Nature* **2006**, *440*, 908−912.
(31) Tanaka, I.; Suzuki, M.; Tokito, S. *Jpn. J. Appl. Phys., Part 1* **2003**, *42*, 2737−2740.
(32) Tokito, S.; Iijima, T.; Tsuzuki, T.; Sato, F. *Appl. Phys. Lett.* **2003**, *83*, 2459−2461.
(33) Xu, Y.; Peng, J.; Jiang, J.; Xu, W.; Yang, W.; Cao, Y. *Appl. Phys. Lett.* **2005**, *87*, 193502−3.
(34) Zhang, Y.; Cheng, G.; Zhao, Y.; Hou, J.; Liu, S. *Appl. Phys. Lett.* **2005**, *86*, 011112−3.
(35) Lamansky, S.; Djurovich, P.; Murphy, D.; Abdel-Razzaq, F.; Kwong, R.; Tsyba, I.; Bortz, M.; Mui, B.; Bau, R.; Thompson, M. E. *Inorg. Chem.* **2001**, *40*, 1704−1711.
(36) Polson, M.; Fracasso, S.; Bertolasi, V.; Ravaglia, M.; Scandola, F. *Inorg. Chem.* **2004**, *43*, 1950−1956.
(37) Dixon, I. M.; Collin, J. P.; Sauvage, J. P.; Flamigni, L.; Encinas, S.; Barigelletti, F. *Chem. Soc. Rev.* **2000**, *29*, 385−391.
(38) Hay, P. J. *J. Phys. Chem. A* **2002**, *106*, 1634−1641.
(39) Cummings, S. D.; Eisenberg, R. *J. Am. Chem. Soc.* **1996**, *118*, 1949−1960.
(40) Li, J.; Djurovich, P. I.; Alleyne, B. D.; Yousufuddin, M.; Ho, N. N.; Thomas, J. C.; Peters, J. C.; Bau, R.; Thompson, M. E. *Inorg. Chem.* **2005**, *44*, 1713−1727.
(41) Nazeeruddin, M. K.; Humphry-Baker, R.; Berner, D.; Rivier, S.; Zuppiroli, L.; Graetzel, M. *J. Am. Chem. Soc.* **2003**, *125*, 8790−8797.
(42) Lee, C. L.; Das, R. R.; Kim, J. J. *Chem. Mater.* **2004**, *16*, 4642−4646.
(43) Dedeian, K.; Shi, J.; Forsythe, E.; Morton, D. C.; Zavalij, P. Y. *Inorg. Chem.* **2007**, *46*, 1603−1611.
(44) Wu, L. L.; Yang, C. H.; Sun, I. W.; Chu, S. Y.; Kao, P. C.; Huang, H. H. *Organometallics* **2007**, *26*, 2017−2023.
(45) Chin, C. S.; Eum, M. S.; Kim, S. Y.; Kim, C.; Kang, S. K. *Eur. J. Inorg. Chem.* **2007**, 372−375.
(46) Laskar, I. R.; Hsu, S. F.; Chen, T. M. *Polyhedron* **2005**, *24*, 189−200.
(47) Lo, S. C.; Shipley, C. P.; Bera, R. N.; Harding, R. E.; Cowley, A. R.; Burn, P. L.; Samuel, I. D. W. *Chem. Mater.* **2006**, *18*, 5119−5129.
(48) Mak, C. S. K.; Hayer, A.; Pascu, S. I.; Watkins, S. E.; Holmes, A. B.; Kohler, A.; Friend, R. H. *Chem. Commun.* **2005**, 4708−4710.
(49) Browne, W. R.; Hage, R.; Vos, J. G. *Coord. Chem. Rev.* **2006**, *250*, 1653−1668.

Furthermore, for the first time, we report the full electrochemical behavior of iridium(III) bis(4,6-difluorophenyl)-pyridinato-*N*,$C^{2'}$)picolinate (FIrpic) in different solvents and compare the properties of our complexes to it. In addition, we fabricated electroluminescent devices that show a better color point than FIrpic itself, which is a common standard for blue emission.

Experimental Section

Photophysics. Absorption spectra were measured on a Varian Cary 5000 double-beam UV−vis−NIR spectrometer and baseline corrected. Steady-state emission spectra were recorded on a HORIBA Jobin-Yvon IBH FL-322 Fluorolog 3 spectrometer equipped with a 450 W xenon arc lamp, double-grating excitation and emission monochromators (2.1 nm/mm dispersion; 1200 grooves/mm), and a Hamamatsu R928 photomultiplier tube or a TBX-4-X single-photon-counting detector. Emission and excitation spectra were corrected for source intensity (lamp and grating) and emission spectral response (detector and grating) by standard correction curves. Time-resolved measurements were performed using the time-correlated single-photon counting (TCSPC) option on the Fluorolog 3. NanoLEDs (295 or 402 nm; fwhm < 750 ps) with repetition rates between 10 kHz and 1 MHz were used to excite the sample. The excitation sources were mounted directly on the sample chamber at 90° to a double-grating emission monochromator (2.1 nm/mm dispersion; 1200 grooves/mm) and collected by a TBX-4-X single-photon-counting detector. The photons collected at the detector are correlated by a time-to-amplitude converter (TAC) to the excitation pulse. Signals were collected using an IBH Data Station Hub photon counting module, and data analysis was performed using the commercially available DAS6 software (HORIBA Jobin Yvon IBH). The goodness of fit was assessed by minimizing the reduced chi squared function (χ^2) and visual inspection of the weighted residuals. Luminescence quantum yields (Φ_{em}) were measured in optically dilute solutions (O.D. < 0.1 at excitation wavelength) and compared to reference emitters by the following equation[50]

$$\Phi_x = \Phi_r \left[\frac{A_r(\lambda_r)}{A_x(\lambda_x)}\right]\left[\frac{I_r(\lambda_r)}{I_x(\lambda_x)}\right]\left[\frac{n_x^2}{n_r^2}\right]\left[\frac{D_x}{D_r}\right]$$

where A is the absorbance at the excitation wavelength (λ), I is the intensity of the excitation light at the excitation wavelength (λ), n is the refractive index of the solvent, D is the integrated intensity of the luminescence, and Φ is the emission quantum yield. The subscripts r and x refer to the reference and sample, respectively. All quantum yields were performed at an identical excitation wavelength for the sample and reference, canceling the $I(\lambda_r)/I(\lambda_x)$ term in the equation. All iridium complexes were measured against quinine bisulfate in 1.0 N sulfuric acid as reference ($\Phi = 0.546$).[50] All solvents were spectrometric grade, and all solutions were filtered through a 0.2 μm syringe filter before measurement. Deaerated samples were prepared by the freeze−pump−thaw technique.

Cyclic Voltammetry. Cyclic voltammetry (CV) was performed in a gas-tight single-compartment three-electrode cell using a Voltalab 40 system from Radiometer Analytical which consists of a PGZ301 potentiostat and Voltamaster 4 software. The working electrode was a Pt disc, the counter electrode was a Pt wire, and a Ag wire was used as a pseudoreference electrode. CVs were elucidated and compared using IGOR. All glassware was dried prior to use. The compounds (electrolyte,[51] analyte, and reference[52]) were placed in a Schlenk flask that was then evacuated and heated with a heat gun to eliminate any moisture and oxygen that had entered during addition. The flask was then evacuated and filled three times with dry $N_{2(g)}$. The solvent[53] was added via syringe directly to the sealed Schlenk flask; the solution was sonicated if necessary and then degassed for 10 min (5 min for CH_2Cl_2) with a gentle stream of dry N_2. After degassing, the solution was added, via syringe, to the electrochemical cell under a positive N_2 pressure and the electrodes then added. The solution was kept under a positive N_2 pressure during the measurements, but no flow was allowed through the cell.

X-ray Crystallography. Data sets were collected with a Nonius KappaCCD diffractometer, equipped with a rotating anode generator. Programs used were as follows: data collection COLLECT,[54] data reduction Denzo-SMN,[55] absorption correction SORTAV[56,57] and Denzo,[58] structure solution SHELXS-97,[59] structure refinement SHELXL-97,[60] and graphics SCHAKAL.[61]

CCDC 623520 (**4e**), 623521 (**4c**), 642606 (**4f**), 642607 (**4g′**), 642608 (**4g″**), and 642787 (**4h**) contain the supplementary crystallographic data for this paper. These data can be obtained free of charge at www.ccdc.cam.ac.uk/conts/retrieving.html.[62]

Device Preparation. LED devices were prepared by vacuum evaporation of the materials at a base pressure of about 10^{-7} mbar. The deposition speed was below 0.1 nm/s, and the layer thickness was checked by quartz balances. The ITO-covered glass substrates contained 16 identical OLEDs of 20 mm^2 each. The finished devices were encapsulated to protect the OLED layer from oxygen and moisture. IVL measurements were performed with a Keithley 2400 source meter and a "LMT L 1009" photometer from LMT Lichtmesstechnik GmbH, Berlin. Spectra were recorded by a Photo Research "SpectraScan" PR 705 spectrophotometer. The luminance values were measured at normal incidence, and the total flux was estimated by assuming a Lambertian distribution.

Synthesis and Characterization. All reagents were analytical grade and used as received. Solvents were purified according to the standard procedures.[63] All reactions were performed under inert atmosphere (Schlenk-line techniques), except where noted. Compounds **3**[10,64] and **4b**[10] were prepared according to the literature procedures. Column chromatography (CC) was performed with silica gel 60 (particle size 63−200 μm, 230−400 mesh, Merck) using common flash procedures.[65] Melting points were measured on a Stuart SMP10 melting point apparatus and are uncorrected.

(50) Eaton, D. F. *Pure Appl. Chem.* **1988**, *60*, 1107−1114.
(51) Tetrabutyl ammonium hexafluorophosphate, >99.0% purity, was dried at 130 °C and stored in a closed vial in a dessicator between experiments.
(52) Usually ferrocene ($FeCp_2$) or decamethylferrocene ($FeCp^*_2$).
(53) Acetonitrile was freshly distilled from P_2O_5, CH_2Cl_2 was freshly distilled from CaH_2, and THF was freshly distilled from Na/benzophenone ketyl radical.
(54) Nonius B. V., 1998.
(55) Otwinowski, Z.; Minor, W. In *Macromolecular Crystallography, Part A*; Academic Press Inc.: San Diego, 1997; Vol. 276, pp 307−326.
(56) Blessing, R. H. *Acta Crystallogr., Sect. A* **1995**, *51*, 33−38.
(57) Blessing, R. H. *J. Appl. Crystallogr.* **1997**, *30*, 421−426.
(58) Otwinowski, Z.; Borek, D.; Majewski, W.; Minor, W. *Acta Crystallogr., Sect. A* **2003**, *59*, 228−234.
(59) Sheldrick, G. M. *Acta Crystallogr., Sect. A* **1990**, *46*, 467−473.
(60) Sheldrick, G. M. Universität Göttingen: Göttingen, Germany, 1997.
(61) Keller, E. Universität Freiburg, 1997.
(62) Or from the Cambridge Crystallographic Data Centre, 12 Union Road, Cambridge CB2 1EZ, U.K. Fax: +44(1223)336-033. E-mail: deposit@ccdc.cam.ac.uk.
(63) Perrin, D. D.; Armarego, W. L. F.; Perrin, D. R. *Purification of Laboratory Chemicals*, 2nd ed.; Pergamon Press: New York, 1980.
(64) Garces, F. O.; King, K. A.; Watts, R. J. *Inorg. Chem.* **1988**, *27*, 3464−3471.
(65) Still, W. C.; Kahn, M.; Mitra, A. *J. Org. Chem.* **1978**, *43*, 2923−2925.

NMR spectra were recorded on an ARX 300 or an AMX 400 from Bruker Analytische Messtechnik (Karlsruhe, Germany). The ^{1}H NMR chemical shifts (δ) of the signals are given in ppm and referenced to residual protons in the deuterated solvents: chloroform-d_1 (7.26 ppm), dimethyl sulfoxide-d_6 (2.50 ppm), or acetone-d_6 (2.09 ppm). The ^{19}F NMR chemical shifts are referenced to $CFCl_3$ (0.00 ppm) as an internal standard. The signal splittings are abbreviated as follows: s = singlet, d = doublet, t = triplet, q = quartet, m = multiplet. All coupling constants (J) are given in Hertz (Hz). Mass spectrometry and elemental (CHN) analyses were performed in the Department of Chemistry, University of Münster. Electrospray ionization (ESI) mass spectra were recorded on a Bruker Daltonics (Bremen, Germany) MicroTof with loop injection. Elemental analysis was provided by Mikroanalytisches Labor Beller (Göttingen, Germany).

(Pyridine-2-yl)amidrazone (1).[66] After melting 10.4 g (0.10 mol) of 2-cyanopyridine with gentle heating, 5.3 mL (5.5 g, 0.11 mol) of hydrazine monohydrate was added, yielding a cloudy mixture. Ethanol (~5 mL) was added until the mixture became clear, and the resulting solution was stirred overnight at room temperature, causing a gel-like product to form. All solvents were removed under reduced pressure, and the solid was suspended in petroleum ether (50 mL), cooled in an ice bath, and filtered, washing with cold petroleum ether, yielding 9.9 g (73%) of the amidrazone. The solid could be used without further purification or crystallized from toluene. Mp: 94−96 °C (lit.[66] 95−96 °C). ^{1}H NMR ($CDCl_3$, 300 MHz): δ 8.50 (d, 1H, J = 4.1 Hz), 8.00 (d, 1H, J = 8.0 Hz), 7.67 (t, 1H, J = 6.2 Hz), 7.24 (d, 1H, J = 6.2 Hz), 5.39 (s, 2H, NH_2), 4.60 (s, 2H, NH_2).

2-(5-R-2*H*-1,2,4-Triazol-3-yl)pyridine (2a−h). General Procedure.[67] In a flame-dried, nitrogen-purged 30 mL Schlenk tube were placed (pyridine-2-yl)amidrazone (2.0 g, 15 mmol) and sodium carbonate (1.6 g, 15 mmol). The flask was evacuated and gently heated. After cooling, the flask was purged with nitrogen. Next, 15 mL of dry dimethylacetamide (DMAA) and 5 mL of dry THF were added, yielding a pale yellow suspension that was cooled to 0 °C. In a separate, dry 10 mL Schlenk flask, 15 mmol of the appropriate acid chloride was dissolved in 5 mL of DMAA. This solution was then added to precooled amidrazone mixture dropwise, which caused it to turn bright yellow. The mixture was slowly warmed to room temperature and stirred for additional 5 h, yielding a thick yellow mixture. The contents were filtered, the solid was washed with water and EtOH, and the resulting pale yellow solid was allowed to air dry. The solid was suspended in 20 mL of ethylene glycol and heated to 190 °C for 30 min, yielding a pale yellow solution. Upon cooling to room temperature, a white solid formed and was collected on a glass frit, washing with deionized water. The solid was dried under vacuum and used without further purification.

2-(5-Methyl-2*H*-1,2,4-triazol-3-yl)pyridine (2a).[68] Acetyl chloride. White solid. Yield: 43%. Mp: 162−165 °C (lit.[68] 163−165 °C). ^{1}H NMR (300 MHz, DMSO): δ 8.78 (d, 1H, J = 3.6 Hz), 8.17 (d, 1H, J = 7.7 Hz), 8.06 (t, 1H, J = 6.6 Hz), 7.58 (m, 1H), 3.54 (s, 3H).

2-(5-Phenyl-2*H*-1,2,4-triazol-3-yl)pyridine (2b). Benzoyl chloride. Yield: 63%. Mp: 212−214 °C (lit.[69] 212 °C). ^{1}H NMR (300 MHz, DMSO): δ 8.73 (d, 1H, J = 4.3 Hz), 8.18 (d, 1H, J = 7.8 Hz), 8.10 (d, 1H, J = 7.0 Hz), 8.02 (t, 1H, J = 7.6 Hz), 7.60−7.40 (m, 4H).

2-(5-*p*-Tolyl-2*H*-1,2,4-triazol-3-yl)pyridine (2c). 4-Methylbenzoyl chloride. Off-white powder. Yield: 97%. Mp: 203−204 °C (lit.[69] 202 °C). ^{1}H NMR (300 MHz, DMSO): δ 8.71 (d, 1H, J = 4.8 Hz), 8.16 (d, 1H, J = 7.8 Hz), 8.05−7.95 (m, 3H), 7.52 (dd, 1H, J = 5.3 Hz, J = 7.0 Hz), 7.31 (d, 1H, J = 8.1 Hz), 2.36 (s, 3H).

2-(5-(4-Methoxyphenyl)-2*H*-1,2,4-triazol-3-yl)pyridine (2d). 4-Anisoyl chloride. Off-white powder. Yield: 58%. Mp: 183−185 °C. ^{1}H NMR (300 MHz, DMSO): δ 8.70 (d, 1H, J = 4.4 Hz), 8.16 (d, 1H, J = 7.8 Hz), 8.04 (d, 2H, J = 8.6 Hz), 7.97 (d, 1H, J = 7.5 Hz), 7.50 (dd, 1H, J = 5.4 Hz, J = 5.8 Hz), 7.06 (d, 2H, J = 8.5 Hz), 3.81 (s, 1H).

2-(5-(Perfluorophenyl)-2*H*-1,2,4-triazol-3-yl)pyridine (2e). Pentafluorobenzoyl chloride. Tan solid. Yield: 60%. The product could be used without further purification, or analytical purity could be obtained by sublimation (120 °C, oil pump) to yield a white solid. Mp: >195 °C (dec). ^{1}H NMR (300 MHz, DMSO): δ 8.75 (d, 1H, J = 4.4 Hz), 8.11 (d, 1H, J = 7.8 Hz), 8.03 (dt, 1H, J = 1.5 Hz, J = 7.8 Hz), 7.57 (dd, 1H, J = 5.2 Hz, J = 6.3 Hz).

2-(5-(2,6-difluorophenyl)-2*H*-1,2,4-triazol-3-yl)pyridine (2f). 2,6-Difluorobenzoyl chloride. Off-white powder. Yield: 45%. Mp: 181−183 °C. ^{1}H NMR (300 MHz, DMSO): δ 9.18 (s, 1H), 8.74 (d, 1H, J = 4.3 Hz), 8.12 (d, 1H, J = 7.8 Hz), 8.01 (t, 1H, J = 7.6 Hz), 7.60 (m, 2H), 7.28 (t, 2H, J = 8.1 Hz).

2-(5-(3,5-Difluorophenyl)-2*H*-1,2,4-triazol-3-yl)pyridine (2g). 3,5-Difluorobenzoyl chloride. Off-white powder. Yield: 68%. Mp: 254−257 °C. ^{1}H NMR (300 MHz, DMSO): δ 15.09 (s, 1H), 7.68−7.59 (m, 1H), 8.18 (d, 1H, J = 7.8 Hz), 8.04 (dt, 1H, J = 1.1 Hz, J = 7.7 Hz), 7.75−7.52 (m, 3H), 7.36 (t, 1H, J = 9.3 Hz).

2-(5-(4-Fluorophenyl)-2*H*-1,2,4-triazol-3-yl)pyridine (2h). 4-Fluorobenzoyl chloride. Off-white powder. Yield: 72%. Mp: 241−243 °C. ^{1}H NMR (300 MHz, DMSO): δ 14.90 (s, 1H), 8.73 (d, 1H, J = 4.3 Hz), 8.21−8.07 (m, 3H), 8.02 (dt, 1H, J = 7.8 Hz), 7.55 (dd, 1H, J = 6.6 Hz), 7.35 (t, 2H, J = 8.8 Hz).

General Procedure for the Synthesis of the Iridium Complexes (4a−h). A 0.2 mmol (1 equiv) amount of $[(F_2ppy)_2Ir(\mu\text{-}Cl)]_2$ and 0.44 mmol (2.2 equiv) of the corresponding pyridinetriazole (pta) were stirred in 15 mL of CH_2Cl_2 and 5 mL of EtOH at room temperature or reflux for 16 h under nitrogen. Upon completion of the reaction (TLC), all solvents were removed under reduced pressure and the resulting yellow solid was chromatographed on silica gel (CC) and crystallized where appropriate.

$(F_2ppy)_2Ir(pta)Me$ (4a). CC: 95/5 CH_2Cl_2/EtOH. Yield: 58%. ^{1}H NMR (300 MHz, CD_2Cl_2): δ 8.26 (dd, 2H, J = 8.3 Hz, J = 16.1 Hz), 8.11 (d, 1H, J = 8.0 Hz), 7.84 (dt, 1H, J = 1.6 Hz, J = 7.8 Hz), 7.78−7.68 (m, 4H), 7.57 (d, 1H, J = 5.0 Hz), 7.11 (ddd, 1H, J = 1.4 Hz, J = 5.5 Hz, J = 7.4 Hz), 7.0 (ddd, 1H, J = 1.4 Hz, J = 5.8 Hz, J = 7.3 Hz), 6.95 (ddd, 1H, J = 1.4 Hz, J = 5.8 Hz, J = 7.3 Hz), 6.50 (dddd, 2H, J = 2.4 Hz, J = 9.3 Hz, J = 12.8 Hz), 5.85 (dd, 1H, J = 2.4 Hz, J = 8.5 Hz), 5.74 (dd, 1H, J = 2.3 Hz, J = 8.7 Hz), 2.37 (s, 3H). ^{19}F{^{1}H} NMR (282 MHz, CD_2Cl_2/$CFCl_3$): δ −108.0 (d, 1F, J = 11.4 Hz), −108.4 (d, 1F, J = 11.4 Hz), −109.9 (d, 1F, J = 11.5 Hz), −110.4 (d, 1F, J = 10.4 Hz). MS (ESI+, MeOH): m/z 715.1 ([M − F + 2H]$^+$, 100), 733.1 ([M + H]$^+$, 100), 755.1 ([M + Na]$^+$). HRMS calcd for $C_{30}H_{19}F_4IrN_6$, 733.1311 ([M + H]$^+$); found, 733.1297. Anal. Calcd for $C_{30}H_{19}F_4IrN_6$: C, 49.24; H, 2.62; N, 11.49. Found: C, 48.88; H, 2.53; N, 11.36.

$(F_2ppy)_2Ir(pta)PhMe$ (4c). CC: 9/1 CH_2Cl_2/MeCN. Crystals were grown by slow evaporation of CH_2Cl_2 from a CH_2Cl_2/hexane solution. Yield: 87%. ^{1}H NMR (300 MHz, $CDCl_3$): δ 8.26 (t, 1

(66) Case, F. H. *J. Org. Chem.* **1965**, *30*, 931−933.
(67) Fanni, S.; Keyes, T. E.; O'Connor, C. M.; Hughes, H.; Wang, R. Y.; Vos, J. G. *Coord. Chem. Rev.* **2000**, *208*, 77−86.
(68) Hage, R.; Prins, R.; Haasnoot, J. G.; Reedijk, J.; Vos, J. G. *J. Chem. Soc., Dalton Trans.* **1987**, 1389−1395.
(69) Potts, K. T. *J. Chem. Soc.* **1954**, 3461−3464.

H, $J = 10.2$ Hz), 8.10 (d, 1H, $J = 7.6$ Hz), 7.92 (t, 1H, $J = 7.7$ Hz), 7.84 (m, 1H), 7.78−7.65 (m, 3H), 7.47 (d, 1H, $J = 5.8$ Hz), 7.24−7.14 (m, 3H), 6.98 (t, 1H, $J = 6.3$ Hz), 6.90 (t, 1H, $J = 6.3$ Hz), 6.50 (ddt, 2H, $J = 2.3$ Hz, $J = 9.1$ Hz, $J = 12.1$ Hz), 5.76 (ddd, 1H, $J = 2.3$ Hz, $J = 8.5$ Hz, $J = 17.8$ Hz), 2.34 (s, 3H). $^{19}F\{^1H\}$ NMR (282 MHz, $CD_2Cl_2/CFCl_3$): δ −107.9 (d, 1F, $J =$ 11.3 Hz), −108.4 (d, 1F, $J = 11.3$ Hz), −109.8 (d, 1F, $J = 11.1$ Hz), −110.4 (d, 1F, $J = 10.6$ Hz). MS (ESI+, MeOH): *m*/*z* 791.2 ($[M - F + 2H]^+$, 2), 809.2 ($[M + H]^+$, 100), 831.4 ($[M + Na]^+$, 5). HRMS calcd for $C_{36}H_{23}F_4IrN_6$, 809.1624 ($[M + H]^+$); found, 809.1593. Anal. Calcd for $C_{36}H_{23}F_4IrN_6$: C, 53.53; H, 2.87; N, 10.40. Found: C, 53.67; H, 2.88; N, 10.48.

$(F_2ppy)_2Ir(pta)PhOMe$ (4d). CC: 9/1 CH_2Cl_2/MeCN. Yield: 69%. ^1H NMR (300 MHz, CD_2Cl_2): δ 8.27 (dd, 2H, $J = 8.4$ Hz, $J = 15.7$ Hz), 8.05 (d, 2H, $J = 7.9$ Hz), 7.92 (t, 1H, $J = 7.7$ Hz), 7.84 (d, 1H, $J = 4.9$ Hz), 7.8−7.7 (m, 3H), 7.57 (d, 1H, $J = 6.0$ Hz), 7.17 (t, 1H, $J = 5.9$ Hz), 7.1−6.8 (m, 4H), 6.53 (dddd, 2H, $J = 2.4$ Hz, $J = 7.3$ Hz, $J = 9.4$ Hz, $J = 12.6$ Hz), 5.85 (dd, 1H, $J = 2.3$ Hz, $J = 8.4$ Hz), 5.78 (dd, 1H, $J = 2.3$ Hz, $J = 8.7$ Hz), 3.82 (s, 3H). $^{19}F\{^1H\}$ NMR (282 MHz, $CD_2Cl_2/CFCl_3$): δ −107.9 (d, 1F, $J = 11$ Hz), −108.5 (d, 1F, $J = 7.7$ Hz), −109.8 (d, 1F, $J = 11$ Hz), −110.4 (d, 1F, $J = 8$ Hz). MS (ESI+, MeOH): *m*/*z* 825.2 ($[M + H]^+$, 100), 847.1 ($[M + Na]^+$, 5). HRMS calcd for $C_{36}H_{23}F_4IrN_6O$, 825.1573 ($[M + H]^+$); found, 825.1554. Anal. Calcd for $C_{36}H_{23}F_4IrN_6O{\cdot}0.5CH_2Cl_2$: C, 50.95; H, 2.77; N, 9.63. Found: C, 51.12; H, 3.00; N, 9.74.

$(F_2ppy)_2Ir(pta)F_5Ph$ (4e). CC: 9/1 CH_2Cl_2/MeCN. Yield: 69%. Single crystals (plates) were grown by slow evaporation of CH_2Cl_2 from a CH_2Cl_2/hexane solution. ^1H NMR (300 MHz, CD_2Cl_2): δ 8.3−8.2 (m, 3H), 7.92 (dt, 1H, $J = 1.5$ Hz, $J = 7.7$ Hz), 7.82 (d, 1H, $J = 4.8$ Hz), 7.79−7.70 (m, 3H), 7.62 (d, 1H, $J = 5.0$ Hz), 7.22 (ddd, 1H, $J = 1.4$ Hz, $J = 5.5$ Hz, $J = 7.4$ Hz), 7.03 (ddd, 1H, $J = 1.4$ Hz, $J = 5.4$ Hz, $J = 7.0$ Hz), 6.97 (ddd, 1H, $J = 1.4$ Hz, $J = 5.9$ Hz, $J = 7.3$ Hz), 6.56 (ddd, 1H, $J = 2.4$ Hz, $J = 9.3$ Hz, $J = 12.6$ Hz), 6.48 (ddd, 1H, $J = 2.4$ Hz, $J = 9.3$ Hz, $J = 12.6$ Hz), 5.89 (dd, 1H, $J = 2.4$ Hz, $J = 8.4$ Hz), 5.78 (dd, 1H, $J = 2.4$ Hz, $J = 8.8$ Hz). $^{19}F\{^1H\}$ NMR (282 MHz, $CD_2Cl_2/CFCl_3$) δ −107.70 (d, 1F, $J = 10.8$ Hz), −108.20 (d, 1F, $J = 11.4$ Hz), −109.72 (d, 1F, $J = 11.6$ Hz), −110.26 (d, 1F, $J = 7.1$ Hz), −140.38 (dd, 2F, $J = 7.3$ Hz, $J = 23.0$ Hz), −155.99 (t, 1F, $J =$ 20.9 Hz), −163.68 (dt, 2F, $J = 6.8$ Hz, $J = 22.3$ Hz). MS (ESI+, MeOH): *m*/*z* 885.1 ($[M + H]^+$, 100), 907.1 ($[M + Na]^+$, 20). HRMS calcd for $C_{35}H_{16}F_9IrN_6$, 907.0816 ($[M + Na]^+$); found, 907.0811. Anal. Calcd for $C_{35}H_{16}F_9IrN_6$: C, 47.57; H, 1.82; N, 9.51. Found: C, 47.17; H, 2.00; N, 8.95.

$(F_2ppy)_2Ir(pta)2,6FPh$ (4f). CC: 9/1 CH_2Cl_2/MeCN. Yield: 45%. Single crystals (plates) were grown by slow evaporation of CH_2Cl_2 from a CH_2Cl_2/hexane solution. ^1H NMR (300 MHz, CD_2Cl_2): δ 8.26 (t, 3H, $J = 9.0$ Hz), 7.90 (dt, 1H, $J = 1.5$ Hz, $J = 7.7$ Hz), 7.76 (m, 4H), 7.63 (d, 1H, $J = 5.8$ Hz), 7.32 (m,1H), 7.19 (ddd, 1H, $J = 1.4$ Hz, $J = 5.5$ Hz, $J = 7.4$ Hz), 6.98 (m, 4H), 6.51 (dddd, 2H, $J = 2.4$ Hz, $J = 9.3$ Hz, $J = 12.6$ Hz, $J = 22.7$ Hz), 5.86 (dd, 1H, $J = 2.4$ Hz, $J = 8.4$ Hz), 5.76 (dd, 1H, $J = 2.4$ Hz, $J = 8.8$ Hz). $^{19}F\{^1H\}$ NMR (282 MHz, $CD_2Cl_2/CFCl_3$) δ −107.95 (d, 1F, $J = 10.44$ Hz), −108.39 (d, 1F, $J = 10.19$ Hz), −109.95 (d, 1F, $J = 10.45$ Hz), −110.45 (d, 1F, $J = 10.26$ Hz), −112.07 (s, 2F). MS (ESI+, MeOH): *m*/*z* 831.0 ($[M + H]^+$, 100), 853.0 ($[M + Na]^+$, 30). HRMS calcd for $C_{35}H_{19}F_6IrN_6$, 831.1279 ($[M + H]^+$); found, 831.1258. Anal. Calcd for $C_{35}H_{19}F_6IrN_6{\cdot}0.5CH_3CN$: C, 50.85; H, 2.43; N, 10.71. Found: C, 51.38; H, 2.68; N, 10.20.

$(F_2ppy)_2Ir(pta)3,5FPh$ (4g). CC: 9/1 CH_2Cl_2/MeCN. Yield: 54%. ^1H NMR (300 MHz, CD_2Cl_2): δ 8.33−8.20 (m, 3H), 7.91 (dt, 1H, $J = 1.6$ Hz, $J = 7.8$ Hz), 7.82−7.70 (m, 4H), 7.67−7.59 (m, 2H), 7.56 (ddd, 1H, $J = 0.7$ Hz, $J = 1.5$ Hz, $J = 5.8$ Hz), 7.19 (ddd, 1H, $J = 1.4$ Hz, $J = 5.5$ Hz, $J = 7.5$ Hz), 6.97 (dddd, 2H, $J = 1.4$ Hz, $J = 5.9$ Hz, $J = 7.3$ Hz, $J = 13.1$ Hz), 6.73 (tt, 1H, $J = 2.4$ Hz, $J = 9.0$ Hz), 6.54 (dddd, 2H, $J = 2.4$ Hz, $J = 7.4$ Hz, $J = 9.6$ Hz, $J = 12.6$ Hz), 5.84 (dd, 1H, $J = 2.4$ Hz, $J = 8.4$ Hz), 5.77 (dd, 1H, $J = 2.3$ Hz, $J = 8.8$ Hz). $^{19}F\{^1H\}$ NMR (282 MHz, $CD_2Cl_2/CFCl_3$): δ −107.86 (d, 1F, $J = 10.46$ Hz), −108.47 (d, 1F, $J = 10.18$ Hz), −109.88 (d, 1F, $J = 10.48$ Hz), −110.47 (d, 1F, $J = 10.21$ Hz), −111.15 (s, 2F). MS (ESI+, MeOH): *m*/*z* 831.3 ($[M + H]^+$, 100), 853.4 ($[M + Na]^+$, 10). HRMS calcd for $C_{35}H_{19}F_6IrN_6$, 831.1279 ($[M + H]^+$); found, 831.1263. Anal. Calcd for $C_{35}H_{19}F_6IrN_6$: C, 50.66; H, 2.31; N, 10.13. Found: C, 51.19; H, 2.80; N, 9.81.

$(F_2ppy)_2Ir(pta)4FPh$ (4h). CC: 95/5 CH_2Cl_2/MeCN. Yield: 65%. Single crystals (plates) were grown by slow evaporation of CH_2Cl_2 from a CH_2Cl_2/hexane solution. ^1H NMR (300 MHz, CD_2Cl_2): δ 8.26 (m, 3H), 8.07 (m, 2H), 7.90 (dt, 1H, $J = 1.5$ Hz, $J = 7.8$ Hz), 7.81 (d, 1H, $J = 5.8$ Hz), 7.75 (m, 3H), 7.57 (d, 1H, $J = 5.8$ Hz), 7.16 (ddd, 1H, $J = 1.4$ Hz, $J = 5.6$ Hz, $J = 7.1$ Hz), 7.00 (m, 4H), 6.53 (dddd, 2H, $J = 2.3$ Hz, $J = 7.3$ Hz, $J = 9.4$ Hz, $J = 12.5$ Hz), 5.84 (dd, 1H, $J = 2.3$ Hz, $J = 8.4$ Hz), 5.77 (dd, 1H, $J = 2.3$ Hz, $J = 8.8$ Hz). $^{19}F\{^1H\}$ NMR (282 MHz, $CD_2Cl_2/CFCl_3$) δ −107.94 (d, 1F, $J = 10.46$ Hz), −108.56 (d, 1F, $J =$ 10.10 Hz), −109.94 (d, 1F, $J = 10.38$ Hz), −110.51 (d, 1F, $J =$ 10.13 Hz), −115.14 (s, 1F). MS (ESI+, MeOH): *m*/*z* 813.4 ($[M + H]^+$, 100), 835.4 ($[M + Na]^+$, 4). HRMS calcd for $C_{35}H_{20}F_5IrN_6$, 813.1373 ($[M + H]^+$); found, 813.1351. Anal. Calcd for $C_{35}H_{20}F_5IrN_6$: C, 51.78; H, 2.48; N, 10.35. Found: C, 52.05; H, 2.78; N, 10.20.

Results and Discussion

Synthesis and Characterization. Scheme 1 shows the general method for the synthesis of the iridium complexes (**4a**−**h**). The triazoles[70−72] (**2a**−**h**) were synthesized in three steps from 2-cyanopyridine: first by reaction with hydrazine monohydrate to form amidrazone **1** followed by treatment with the corresponding substituted acyl chloride in basic media. The last step involves heating the product in ethylene glycol at 190 °C for 1 h, giving the 1,2,4-triazoles in 50−70% yield.

The substituted triazoles and dichloro-bridged iridium complex[64] (**3**) were then stirred together in a mixture of dichloromethane/ethanol (3/1) for 5−6 h. The crude products were purified via chromatography on silica gel, affording complexes **4a**−**h** in 50−60% yield. Complex **4b** and related analogs were previously synthesized in our laboratories.[10] Characterization of all the products was performed using ^1H NMR, ^{19}F NMR, high-resolution mass spectrometry, and elemental analysis.

Single crystals of complexes **4c** and **4e**−**h** were obtained by slow evaporation of dichloromethane from a dichloromethane/hexanes solution, and X-ray crystallographic analyses were performed. Selected parameters of the molecular

(70) Barigelletti, F.; De Cola, L.; Balzani, V.; Hage, R.; Haasnoot, J. G.; Reedijk, J.; Vos, J. G. *Inorg. Chem.* **1989**, *28*, 4344−4350.
(71) Lempers, H. E. B.; Haasnoot, J. G.; Reedijk, J.; Hage, R.; Weldon, F. M.; Vos, J. G. *Inorg. Chim. Acta* **1994**, *225*, 67−74.
(72) Passaniti, P.; Browne, W. R.; Lynch, F. C.; Hughes, D.; Nieuwenhuyzen, M.; James, P.; Maestri, M.; Vos, J. G. *J. Chem. Soc., Dalton Trans.* **2002**, 1740−1746.

Scheme 1. General Procedure for Synthesis of the Iridium Complexes Presented in This Paper and Their Corresponding Abbreviations; Reference Complex FIrpic Is Also Shown for Clarity

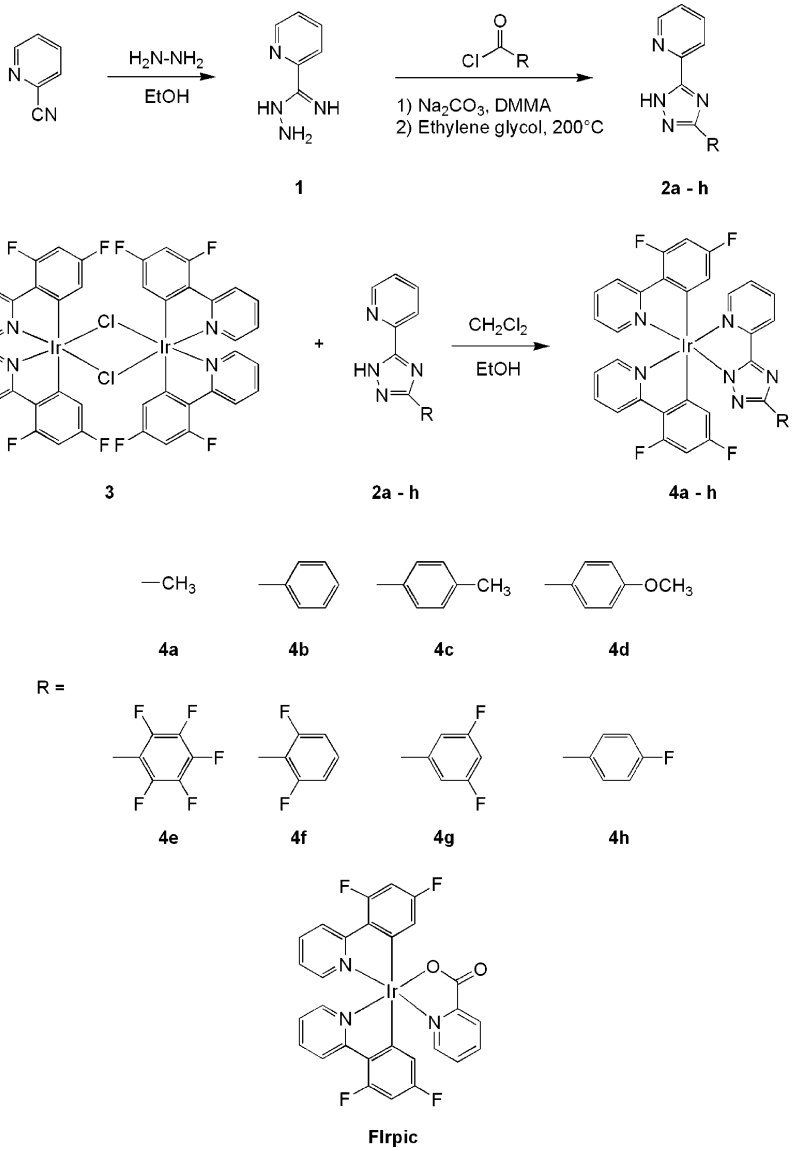

structures are given in Table S2 (see Supporting Information). As shown in Figure 1, all complexes crystallize as distorted octahedrons around the central iridium atom. The difluorophenylpyridine (F_2ppy) ligands have Ir−N bond lengths between 2.023 and 2.042 Å and Ir−C between 1.989 and 2.018 Å (typical Ir−C lengths[16,35,48] 2.00−2.02 Å). The F_2ppy C−C and C−N intraligand bond lengths and angles are within normal ranges expected for cyclometalated Ir(III) complexes.[35] Nitrogens N(21) and N(41) on the F_2ppy ligands are trans to one another, and in complex **4c** they are slightly more skewed from linearity (173.7°) than in **4e** (174.5°).

The Ir−N bonds between the metal center and the pyridine-1,2,4-triazole ligand [Ir(1)−N(1) and Ir(1)−N(8)] are longer if compared to the Ir−N bonds between the metal and the pyridine moiety of the F_2ppy [Ir(1)−N(21) and Ir(1)−N(41)]: in other words, bonds trans to C atoms are longer than bonds trans to N atoms due to the sigma donation of the carbons (trans effect). The most interesting feature of such crystal structures and also the main difference among the complexes is the torsional angle between the triazole ring and the substituted phenyl ring. As can be seen in the case of complexes **4e** and **4f**, due to the steric hindrance of the F atoms in the 2 and 6 positions, the phenyl ring is quite twisted with respect to the triazole ring (64.4° and 84.2°, respectively) while for complexes **4c**, **4g**, and **4h**, this torsional angle is closer to coplanarity (21.7°, 4.6°, and 9.6°, respectively). Crystals of complex **4g** were obtained with two different packing parameters (**4g′** and **4g″**), and some selected parameters for both crystal structures are reported in Table S2. All complexes exhibit the same coordination behavior: the nitrogen of the triazole coordinated to the metal ion is always N8, which is the most basic, and the two phenylpyridines are in a mer configuration.

Absorption and Emission Spectroscopy. The absorption spectra of complexes **4a**−**h** (and FIrpic for comparison) were recorded at room temperature in dichloromethane solutions (Figure 2). The spectra are dominated by transitions falling in two main regions. By comparison with the FIrpic absorption spectrum, the intense bands ($\epsilon \approx 20-60 \times 10^3$

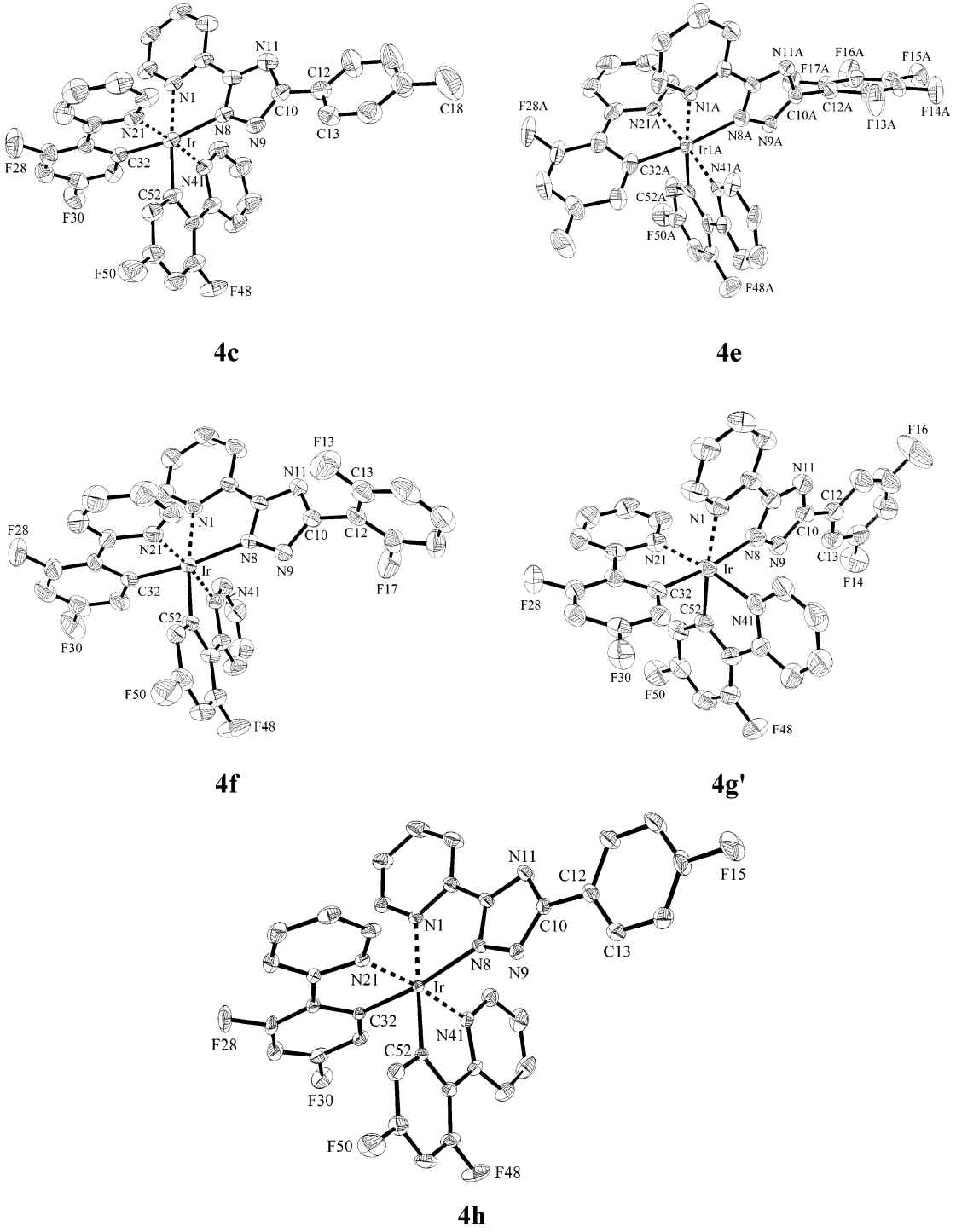

Figure 1. Molecular structures of **4c**, **4e, 4f, 4g′**, and **4h**. Hydrogen atoms and solvent molecules were omitted for clarity.

M^{-1} cm^{-1}) at high energy (<340 nm) are assigned to $\pi-\pi^*$ transitions localized on the coordinated ligands. The highest energy absorptions are due to transitions centered on the F_2ppy ligands, and the shoulder at ~290 nm is attributed to transitions centered on the triazole ligand. Weaker but nonetheless intense transitions ($\epsilon \approx 3-12 \times 10^3$ M^{-1} cm^{-1}) at lower energy (340−450 nm) are due to spin-allowed singlet-to-singlet metal-to-ligand charge-transfer (^{1}MLCT) and spin-forbidden singlet-to-triplet ^{3}MLCT transitions, known for complexes containing heavy atoms such as iridium in which spin−orbit coupling is strong.[73] The main bands and molar extinction coefficients are given in Table 1. Complexes **4b**−**h** show larger extinction coefficients than **4a**, which can be attributed to the increased conjugation due to the phenyl group on the former complexes.

All of the complexes show bright emission at room temperature (Figure 3) in deareated dichloromethane solutions and exhibit photoluminescence spectra with maxima

(73) Chou, P. T.; Chi, Y. *Eur. J. Inorg. Chem.* **2006**, 3319−3332.

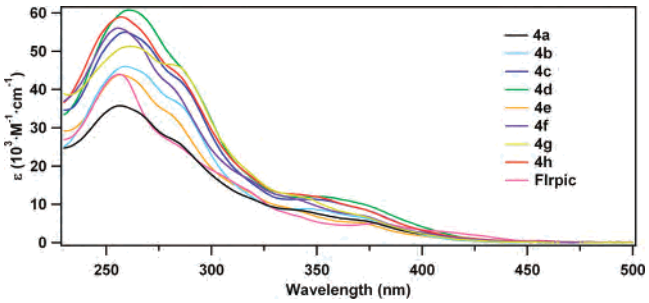

Figure 2. Absorption spectra of complexes **4a**−**h** and FIrpic in CH_2Cl_2 solutions at room temperature.

in the range between 450 and 550 nm. The vibronic structure of the emission bands indicates a large amount of ^{3}LC character, and the excited state is believed to be a mixture of ^{3}LC and ^{3}MLCT states as also confirmed by theoretical studies.[14,35,36,74] The photophysical data of all complexes are collected in Table 1.

The emission spectra of complexes **4a**−**c** and **4e**−**h** all have a very similar shape with an intense high-energy band at around 460 nm, a second less intense band around 490 nm, and a shoulder near 525 nm. Complex **4e** is slightly more blue shifted than the others (458 nm), while for complex **4d** the maximum shifts to 492 nm and the bands at 464 and 525 nm are present only as shoulders, shifting the color point to the green region. This behavior can be explained by the electron-donating character of the methoxy substituent, which raises the energy of the HOMO level of the complex. This complex also has the highest quantum yield among the complexes studied here; blue-emitting complexes generally have lower quantum yields than green-emitting analogs because of the ligand-centered character of the emission.[14,48] Also, by analyzing the spectral shapes, it is observed that complexes **4b**−**d**, bearing electron-donating groups on the triazole ligand, have an emission tail in the green region much higher in intensity with respect to the other complexes. This will influence the emission color coordinates, an important consideration when such complexes are used as OLED dopants. On the basis of these considerations a proper choice of the ligands in the synthesis of such complexes could be useful to achieve narrower (for monochromatic LEDs) or broader (for white-light LEDs) emission spectra.

Emission quantum yields in degassed solutions are relatively high (16−60%), and their extreme oxygen sensitivity is a confirmation of the triplet character of the emission (Table 1). Interestingly, the quantum yields (Φ) of the complexes studied here can be divided into two groups: for complexes **4a**−**d**, **4g**, and **4h** the values are all quite high (>29%), while for complexes **4e** and **4f** the values are remarkably lower (∼16%). Interestingly, the photophysical behavior among the complexes bearing a partially (**4f**−**h**) or fully (**4e**) fluorinated phenyl ring on the triazole ligand seems to correlate quite well with the torsional angle, deduced from the molecular structures, between these two aromatic moieties. The larger the torsional angle, the lower the quantum yield and excited-state lifetime values of the complexes (see Tables 1 and S2). In other words, breaking the conjugation between the triazole and phenyl rings apparently results in a remarkable decrease in the emission intensities and excited-state lifetimes. We believe this effect is related to the nature of the emitting state (vide infra).

The excited-state lifetimes (τ) of complexes **4a**−**h** in deareated dichloromethane solutions scale with the quantum yield values shown by each complex but vary over 1 order of magnitude, from 0.53 to 5 μs, while those of air-equilibrated solutions are all in the narrow range between 130 and 160 ns. All the lifetime decays were found to be monoexponential. The radiative and nonradiative rate constants can be calculated from eqs 1 and 2, respectively, and the results are summarized in Table 1.

$$k_r = \frac{\Phi}{\tau} \quad (1)$$

$$k_{nr} = \frac{(1-\Phi)}{\tau} \quad (2)$$

The radiative rate constants (k_r) calculated for this series vary over a fairly small range and are in line with highly luminescent Ir(III) complexes reported in the literature.[6,16,18] On the other hand, the nonradiative rate constants (k_{nr}) are more instructive. Complexes **4a**−**c**, **4g**, and **4h**, which exhibit similar photophysical properties, have k_r and k_{nr} values in a narrow range. Likewise, if we compare complex **4d** with **4e** and **4f**, the k_r values are similar but **4d** has a much lower value for k_{nr}, while **4e** and **4f** have the highest values among the series, in line with the dramatic differences in excited-state lifetimes and quantum yields for these three complexes. Going from green to blue, the ^{3}MLCT bands approach the ^{3}LC levels and their mixing becomes larger. Due to the low phosphorescence of these ligands, nonradiative decay dominates, thus lowering the emission quantum yields. On the other hand, for our complexes the shift in emission is too small to justify such a different behavior for complexes **4e** and **4f** versus the others.

For iridium(III) complexes, and in general for luminescent transition-metal complexes, the triplet excited states are usually known to reside at energies sufficiently high as not to be deactivated vibronically by low-energy states ("energy-gap law"[39,75,76]). However, a recent study on iridium(III) phenyl-triazole complexes[47] analyzed the correlation between the decrease in the quantum yield with a blue shift in emission energy and suggested that thermally activated, vibrational (nonradiative) decay could be responsible for the quenching of the photoluminescence. In our case, the range of emission quantum yield values reported in Table 1 appears to be mostly related to a distortion from coplanarity between the triazole and substituted phenyl ring connected to it more than to an increase of the electron-withdrawing properties of the substituent on the 1,2,4-triazole moiety. We believe that in the case of compounds **4e** and **4f** the lowest excited

(74) Avilov, I. V.; Minoofar, P.; Cornil, J.; De Cola, L. *J. Am. Chem. Soc.* **2007**, *129*, 8247−8258.
(75) Caspar, J. V.; Kober, E. M.; Sullivan, B. P.; Meyer, T. J. *J. Am. Chem. Soc.* **1982**, *104*, 630−632.
(76) Caspar, J. V.; Meyer, T. J. *Inorg. Chem.* **1983**, *22*, 2444−2453.

Table 1. Absorption and Emission Spectral Data at Room and Low Temperature of Complexes **4a**−**h**[a]

complex	absorbance λ (nm)[b] (ϵ 10^4 M^{-1} cm^{-1})	emission, λ (nm),[c] (rel. int.)	Φ dear.[d]	Φ aerated[d]	τ (μs) deaer.	τ (μs) aerated	k_r (10^5 s^{-1})	k_{nr} (10^5 s^{-1})	emission, λ (nm), at 77 K[c]	τ (μs)[c] at 77 K (rel. wt.)
4a	258 (3.57), 282 (sh, 2.68), 343 (0.83), 374 (0.56), 451 (0.04)	461 (1), 492 (0.88)	0.36	0.047	0.93	0.16	3.9	6.9	451	3.3
4b	258 (4.6), 280 (sh, 3.77), 315 (sh, 1.34), 336 (0.87), 370 (0.66), 452 (0.014)	460 (1), 489 (0.94)	0.37	0.033	1.6	0.15	2.3	3.9	451	3.6
4c	259 (5.50), 281 (sh, 4.39), 315 (sh, 1.73), 337 (sh, 1.12), 370 (0.9), 451 (0.021)	463 (0.98), 492 (1)	0.41	0.025	2.1	0.13	2.0	2.8	451	3.8
4d	261 (6.08), 287 (sh, 4.48), 354 (1.20), 370 (1.03), 451 (0.040)	464 (0.64), 492 (1)	0.59	0.014	5.0	0.13	1.2	0.82	452	3.7 (67%) 8.4 (33%)
4e	257 (4.38), 280 (sh, 3.37), 350 (0.67), 370 (0.52), 451 (0.04)	458 (1), 487 (0.87)	0.16	0.042	0.53	0.15	3.0	15.8	450	3.6
4f	256 (5.60), 282 (sh, 4.02), 315 (sh, 1.73), 342 (1.10), 370 (0.72), 451 (0.031)	460 (1), 490 (0.80)	0.16	0.041	0.60	0.14	2.7	13.7	450	3.6
4g	261 (5.12), 283 (4.63), 315 (sh, 1.98), 346 (1.15), 370 (0.72), 451 (0.025)	459 (1), 488 (0.83)	0.29	0.042	0.99	0.15	2.9	7.1	451	3.6
4h	257 (5.89), 284 (sh, 4.41), 350 (1.25), 370 (0.90), 451 (0.041)	459 (1), 489 (0.87)	0.34	0.028	1.57	0.14	2.1	4.2	451	3.5

[a] All data for complexes in CH_2Cl_2. [b] 'sh' denotes a shoulder. [c] λ_{ex} = 350 nm. [d] Quantum yields are measured versus quinine bisulfate in 1 N H_2SO_4 (λ_{ex} = 350 nm).

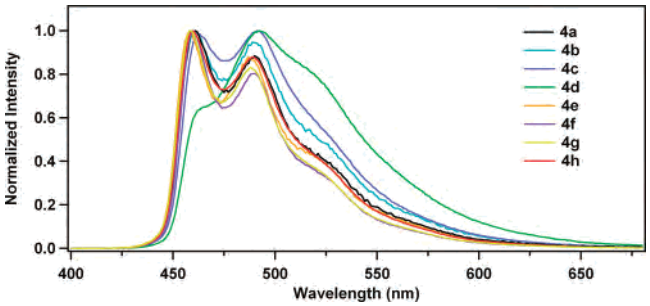

Figure 3. Normalized room-temperature emission spectra of complexes **4a**−**h** in CH_2Cl_2 (λ_{exc} = 350 nm).

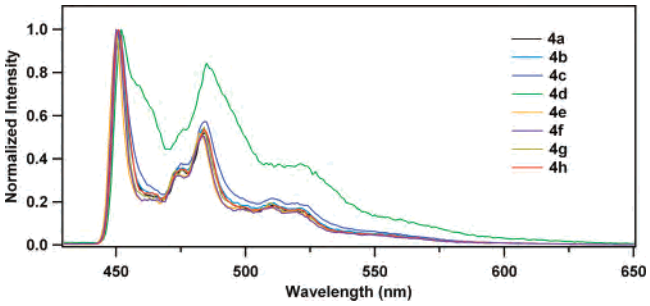

Figure 4. Emission spectra of iridium complexes at 77 K in a butyronitrile glass (λ_{exc} = 350 nm).

state involves the F_2ppy ligands even though for fluorinated derivatives we would expect the lowest excited state to reside on the lower energy triazole ligand. However, due to the large torsional angle between the triazole and the fluorinated phenyl ring (see molecular structure) delocalization is prevented and, therefore there is no electronic coupling between the triazole ring and electron-withdrawing groups. Therefore, in **4e** and **4f** the pyridinetriazole is completely decoupled, thus favoring transitions from the iridium to the F_2ppy ligand, even though the iridium is not as electron rich as in the case of the phenyl derivative **4b**. In the case of electron-donating groups (**4a**, **4c**, and **4d**), the transition is also F_2ppy based because of the donating character of the ligands. This behavior has been supported for some of the complexes by theoretical calculations where the emitting states of **4a** and **4e** were found to be F_2ppy based and that of **4b** was located on the pyridinetriazole.[74]

To gain more insight into the nature of the excited states in these complexes, the emission spectra and excited-state lifetimes were measured at 77 K in butyronitrile glasses. The results are shown in Figure 4 and the data are summarized in Table 1. All complexes show a rigidochromic shift toward the blue when frozen in the glass, giving further evidence for the ^{3}MLCT character of the excited state,[6,39] but the structure of the emission would once again indicate some ^{3}LC contribution. As explained above, the emitting state is likely a mixture of the two. Analogous to the room-temperature emission, complexes **4a**−**c** and **4e**−**h** behave similarly, displaying only small shifts in peak maxima, while **4d** shows a qualitatively similar but much broader profile, especially in the lower energy transitions.

The triplet levels of the complexes were calculated from the 0−0 transitions (E_{0-0}) in the 77 K spectra. Complexes **4a**, **4b**, **4c**, **4g**, and **4h** have almost identical emission at 451 nm (22 173 cm^{-1}, 2.75 eV), while **4e** and **4f** are very slightly blue shifted (22 222 cm^{-1}, 2.76 eV), and the methoxy-substituted **4d** has a 1 nm red shift (22 124 cm^{-1}, 2.75 eV). This gives further support to the theory that donating and withdrawing groups on the pyridinetriazole can lead to color shifts in the emission, although the effects are relatively weak. The weak blue shift of complexes **4e** and **4f** could also be due, as discussed previously, to the electronic decoupling caused by the tilt angle (see molecular structure). Rigidochromic shifts can give information on the emitting states of the complexes, and as in the room-temperature spectra, it is observed that **4d** has a larger fraction of emission in lower energy vibrational bands, even though in all cases at 77 K the peak at ~450 nm is the highest intensity transition. Lifetime values measured at 77 K are all in a narrow range between 3.3 and 3.8 μs, with the exception of **4d** which has a biexponential decay of 3.7 and 8.4 μs. These values indicate that the triplet state is the same for complexes **4a**−**c** and **4e**−**h**, while **4d** has emission from two nonequilibrated states. We are not sure about the reason for this

Table 2. Electrochemical Data for the Ir(III) Complexes in Acetonitrile versus Ferrocene/Ferrocenium

compound	E_{red} (V)	ΔE_{pp}[a] (mV)	E_{red} (V)	ΔE_{pp}[a] (mV)	E_{ox} (V)	ΔE_{pp}[a] (mV)
$Ir(ppy)_3$			−2.67	110	0.33	58
FIrpic	−2.60	105	−2.28	80	0.89	78
4a	[b]		−2.6[b]		1.3[b]	
4b	−2.64	135	−2.38	100	0.95	70
4c	−2.65	108	−2.38	79	0.91	70
4d	−2.66	100	−2.38	84	0.91	74
4e	−2.63[c]	72	−2.34[c]	75	1.02	84
4f	−2.65	80	−2.36	110	0.99	70
4g	−2.63	110	−2.36	95	0.99	75
4h	−2.67	115	−2.38	100	0.97	65

[a] Peak-to-peak separation. [b] Irreversible. [c] Not fully reversible.

behavior, but we believe that due to the strong electron-withdrawing fluorine substituents on the phenylpyridines and the strongly electron-donating methoxy group on the triazole, a ligand-to-ligand charge transfer (LLCT) transition is responsible for the longest lifetime. This state would then be responsible for the broader emission of this complex at room temperature versus the others (see Figure 3). We cannot, however, exclude aggregation phenomena that may also cause the same biexponential decay, even though we are working in very dilute conditions (10^{-6} M).

All these data indicate that (a) the substitution on the triazole represents a small perturbation to the energy levels, (b) the electron-donating or -withdrawing ability of the substituents and even torsional angles can change the emission properties, and (c) the increased broadness in the case of **4d** could be due, besides the MLCT states, to an LLCT state or aggregation phenomena.

Electrochemistry. To better understand the nature of the frontier orbitals as well as probe possible device behavior, cyclic voltammetry (CV) measurements were performed on all complexes reported here (Table 2). Even though FIrpic is a very common dopant for devices, we found very few reports[77] on its electrochemical properties. For the first time we report the reduction behavior of FIrpic in different solvents (Figure 5). As can be seen, both reductions are perfectly reversible in solvents such as THF and acetonitrile, while in dichloromethane even the first reduction is irreversible. The reductions occur on the fluorinated ppy and are scan-rate dependent.

Complexes **4b**−**d** and **4f**−**h** show reversible oxidation and reduction waves; **4e** has a semi-reversible oxidation and reversible reductions, and **4a** does not show any reversible redox processes. As noted previously, for many phenylpyridine Ir(III) complexes the HOMO is mostly localized on the phenyl part of the phenylpyridine ligand and has a large contribution arising from the d atomic orbitals (AOs) of Ir while the LUMO is mostly localized on the pyridine of the phenylpyridine unit. On this basis we expect the first reduction to appear at similar values for all complexes studied and the reduction values should be similar to those of FIrpic. This is confirmed in the data presented in Table 2. The first reduction of all the triazole-containing complexes is 100 mV more negative than that of FIrpic with a spread of 40 mV among them. The 100 mV difference in the first reduction demonstrates the effect of the ancillary pyridine-triazole ligands relative to the picolinate of FIrpic. The first reduction in complexes **4b**−**h** is approximately 400 mV easier than in $Ir(ppy)_3$, which attests the electron-withdrawing capability of fluorine atoms on the F_2ppy units.

The first oxidation potential of FIrpic is slightly lower than those of complexes **4b**−**h** but far higher than for $Ir(ppy)_3$ (Table 2). The small difference between FIrpic and complexes **4b**−**h** indicates that the difluorophenyl-pyridine ligand plays a major role in the oxidation process with some modulation due to the ancillary ligand. The large difference between FIrpic and $Ir(ppy)_3$ similarly confirms the large effect of adding the fluorine atoms to the phenyl rings toward lowering the energy of the HOMO.

The lower reduction potential (less negative) of the studied iridium(III) complexes is compensated by their far higher oxidation potentials, all of which are ∼3 times that of the green-emitting $Ir(ppy)_3$, which we measured here using the same conditions (Table 2). The significant increase in oxidation potentials for complexes **4b**−**h** compensate for the lower reduction potentials. Complex **4e** has the highest oxidation and lowest reduction potential, which agrees with the spectroscopic data showing that it is the bluest emitter. Complex **4d**, the greenest emitter, has almost identical electrochemical signals as the other complexes, possibly indicating that the HOMO−LUMO transition is that at 465 nm (which appears as a shoulder) and not at the peak maximum at 492 nm.

OLED Studies. From the Ir(III) complexes investigated in solution, two of them were selected to construct organometallic light-emitting diodes, OLEDs. The electroluminescent devices were prepared from the materials **4a** and **4e** by sublimation. The device structure was as follows: glass/ITO/hole injection layer of 4,4′,4″-tris(3-methylphenylphenylamino)triphenylamine (m-MTDATA) doped with 2,3,5,6-tetrafluoro-7,7,8,8-tetracyanoquinodimethane (F4-TCNQ) (40 nm)/hole transport layer of undoped MTDATA (10 nm)/emission layer of 4,4′,4″-tri(*N*-carbazolyl)triphenylamine (TCTA) doped with either **4a** or **4e** (25 nm)/hole blocking layer (10 nm)/electron transport layer of 1,3,5-tris[*N*-(phenyl)benzimidazole]benzene (TPBI) (40 nm)/LiF (1 nm)/Al (100 nm). The doping concentration for the iridium emitters was about 8% by weight.

Biasing the devices in normal direction (positive anode, negative cathode) yielded an emission of blue light at the turn-on voltage of about 4.7 V (Table 3; Figure S1b).

The EL spectra of the devices are shown is Figure 6. The emission maxima of complexes **4a** and **4e** in the devices are only very slightly (3 nm) red shifted compared to the emission maxima of the same compounds in dichloromethane solutions. A maximum efficiency of ∼13.5 cd/A was achieved for both complexes, while the power efficiency at 300 cd/m^2 of **4a** was slightly higher (5.5 lm/W) than that of **4e** (4.7 lm/W). High external quantum efficiencies (EQE) were also measured (7.1% for **4a** and 7.4% for **4e**), and the 1931 Commission Internationale de L'Eclairage (x,y) coordinates ($CIE_{x,y}$) coordinates for both complexes displayed a

(77) Muegge, B. D.; Richter, M. M. *Anal. Chem.* **2004**, *76*, 73−77.

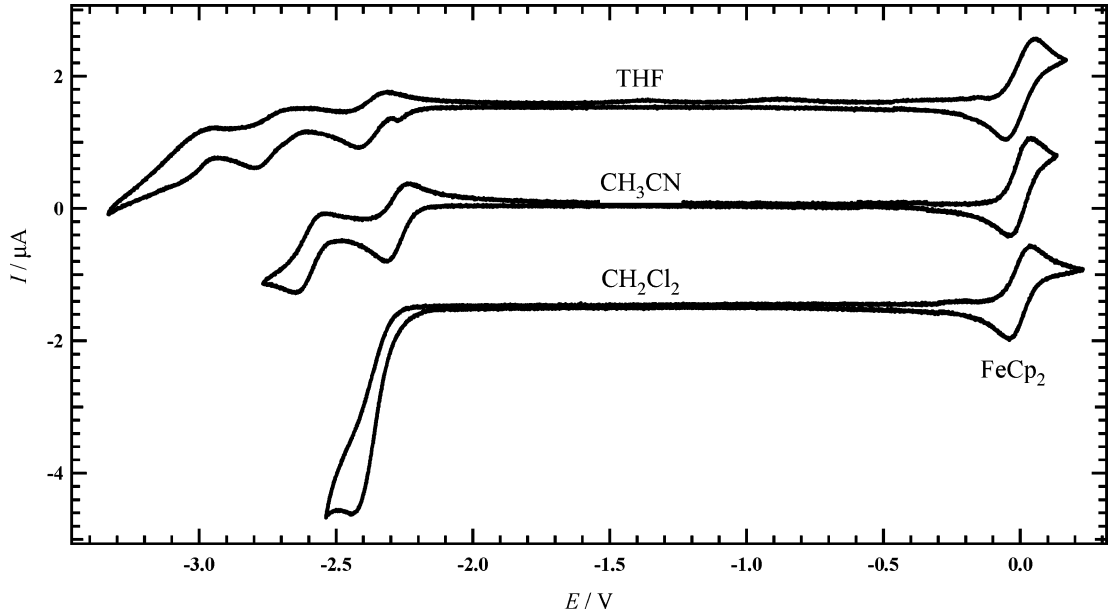

Figure 5. Reduction waves of FIrpic in different solvents. The oxidation wave of ferrocene ($FeCp_2$) is shown and set as zero. Scan rate: 100 mV/s.

Table 3. Device Characteristics for Complexes **4a** and **4e**

emitter	onset voltage (1 cd/m^2) [V]	max efficiency [cd/A]	power efficiency at 300 cd/m^2 [lm/W]	color point	max EQE[a] [%]
4a	4.7	13.4	5.5	0.168, 0.281	7.1
4e	4.7	13.5	4.7	0.170, 0.265	7.4

[a] External quantum efficiency.

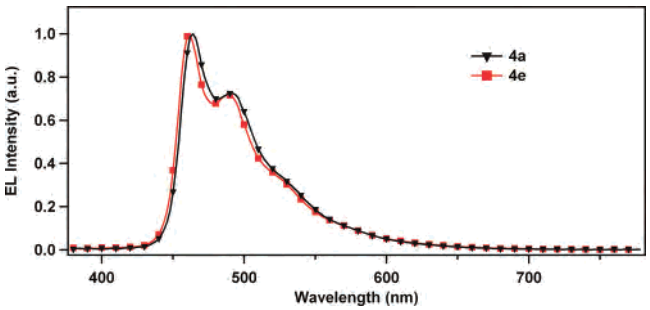

Figure 6. Electroluminescence spectra of the studied devices made with complexes **4a** and **4e**.

blue color which is purer than that reported by FIrpic (0.17, 0.34).[17] As reported for other phosphorescent OLEDs with iridium complexes (see, for example, refs 19, 30, and 78), our devices undergo significant roll-off with increasing current density (Figure S1(a), see Supporting Information), as already reported in the literature.[79] These results are among the best for devices made with similar compounds based on the same heteroleptic (2,4-F_2ppy)Ir((1,2,4-triazol-3-yl)pyridine) moiety[48,80] with an EQE of 4.8% for the bluest device.[80] However, it has to be noted that such results were obtained using solution processing methods for device fabrication, which generally give poorer performance when compared with devices made by vapor deposition.

Nonetheless, devices made with FIrpic still exhibit higher efficiencies,[17] and further optimization of materials and devices is necessary to achieve comparable or better performances. It is interesting to note that the device behavior was very similar for complexes **4a** and **4e**, even though the photoluminescence quantum yields in solution were quite different (0.16 for **4e** vs 0.36 for **4a**), and the electrochemistry of **4a** showed irreversible behavior. The irreversibility would likely manifest itself in the lifetime of the device, and further tests are ongoing to investigate lifetimes and stability of these materials.

Conclusions

We reported the synthesis and photophysical and electrochemical characterization of new Ir(III) complexes based on substituted pyridine-1,2,4-triazole ligands. The complexes were synthesized in good yields and fully characterized. We have shown that by changing the substituents on the triazole fragment we can tune the photophysical properties of the complexes to achieve narrow blue emission. At room temperature, all complexes show bright emission from the green to the blue, depending on the electronic and steric properties of the substituents. In this study, the decrease in emission quantum yields and excited-state lifetimes for complexes **4e** and **4f** seems to be related to the torsional angle between the phenyl and triazole rings, which causes a switch of the lowest MLCT state from the pyridyl-triazole to the phenylpyridines.

Preliminary device tests made with two of these complexes were encouraging and showed high external quantum efficiencies (~7%) together with good blue color points (0.17, 0.27). Moreover, we measured the full electrochemical properties of FIrpic in different solvents and found it to be completely reversible in THF and acetonitrile.

(78) Chang, C. J.; Yang, C. H.; Chen, K.; Chi, Y.; Shu, C. F.; Ho, M. L.; Yeh, Y. S.; Chou, P. T. *Dalton Trans.* **2007**, 1881−1890.
(79) Baldo, M. A.; Adachi, C.; Forrest, S. R. *Phys. Rev. B* **2000**, *62*, 10967−10977.
(80) Zhang, X. J.; Jiang, C. Y.; Mo, Y. Q.; Xu, Y. H.; Shi, H. H.; Cao, Y. *Appl. Phys. Lett.* **2006**, *88*, 051116.

Acknowledgment. The authors would like to acknowledge Philips Research and SENTER (TRIPLED RWC-061-JH-04063-jh)] for supporting this work.

Note Added after ASAP Publication. This article was released ASAP on November 21, 2007, with the incorrect structure for **4h** in Figure 1. The correct version was posted on November 26, 2007.

Supporting Information Available: Crystallographic information files (cif), X-ray crystallographic data for complexes **4b**, **4e**−**h**, and plots of luminescence versus voltage and EQE versus current density for the devices reported. This material is available free of charge via the Internet at http://pubs.acs.org.

IC701110P